Ultradilute self-bound quantum droplets in Bose-Bose mixtures at finite temperature

Jia Wang(王佳), Xia-Ji Liu(刘夏姬), and Hui Hu(胡辉)

Citation: Chin. Phys. B, 2021, 30 (**1**): 010306. DOI: 10.1088/1674-1056/abd2ad
Journal homepage: http://cpb.iphy.ac.cn; http://iopscience.iop.org/cpb

What follows is a list of articles you may be interested in

Effects of a finite number of particles on the thermodynamic properties of a harmonically trapped ideal charged Bose gas in a constant magnetic field

Duan-Liang Xiao(肖端亮), Meng-Yun Lai(赖梦云), Xiao-Yin Pan(潘孝胤)
Chin. Phys. B, 2016, 25 (**1**): 010307. DOI: 10.1088/1674-1056/25/1/010307

Spin-orbit coupled Bose-Einstein condensates with Rydberg-dressing interaction

Lü Hao, Zhu Shao-Bing, Qian Jun, Wang Yu-Zhu
Chin. Phys. B, 2015, 24 (**9**): 090308. DOI: 10.1088/1674-1056/24/9/090308

The effect of s-wave scattering length on self-trapping and tunneling phenomena of Fermi gases in one-dimensional accelerating optical lattices

Jia Wei, Dou Fu-Quan, Sun Jian-An, Duan Wen-Shan
Chin. Phys. B, 2015, 24 (**4**): 040307. DOI: 10.1088/1674-1056/24/4/040307

Dynamical Casimir effect in superradiant light scattering by Bose–Einstein condensate in an optomechanical cavity

Sonam Mahajan, Neha Aggarwal, Aranya B Bhattacherjee, ManMohan
Chin. Phys. B, 2014, 23 (**2**): 020315. DOI: 10.1088/1674-1056/23/2/020315

Novel exact solutions of coupled nonlinear Schrödinger equations with time–space modulation

Chen Jun-Chao, Li Biao, Chen Yong
Chin. Phys. B, 2013, 22 (**11**): 110306. DOI: 10.1088/1674-1056/22/11/110306

SPECIAL TOPIC — Ultracold atom and its application in precision measurement

Ultradilute self-bound quantum droplets in Bose–Bose mixtures at finite temperature*

Jia Wang(王佳), Xia-Ji Liu(刘夏姬), and Hui Hu(胡辉)†

Centre for Quantum Technology Theory, Swinburne University of Technology, Melbourne, Victoria 3122, *Australia*

(Received 28 October 2020; revised manuscript received 9 December 2020; accepted manuscript online 11 December 2020)

We theoretically investigate the finite-temperature structure and collective excitations of a self-bound ultradilute Bose droplet in a flat space realized in a binary Bose mixture with attractive inter-species interactions on the verge of mean-field collapse. As the droplet formation relies critically on the repulsive force provided by Lee–Huang–Yang quantum fluctuations, which can be easily compensated by thermal fluctuations, we find a significant temperature effect in the density distribution and collective excitation spectrum of the Bose droplet. A finite-temperature phase diagram as a function of the number of particles is determined. We show that the critical number of particles at the droplet-to-gas transition increases dramatically with increasing temperature. Towards the bulk threshold temperature for thermally destabilizing an infinitely large droplet, we find that the excitation-forbidden, self-evaporation region in the excitation spectrum, predicted earlier by Petrov using a zero-temperature theory, shrinks and eventually disappears. All the collective excitations, including both surface modes and compressional bulk modes, become softened at the droplet-to-gas transition. The predicted temperature effects of a self-bound Bose droplet in this work could be difficult to measure experimentally due to the lack of efficient thermometry at low temperatures. However, these effects may already present in the current cold-atom experiments.

Keywords: Bose–Einstein condensation, quantum droplet

PACS: 03.75.–b, 03.75.Kk **DOI:** 10.1088/1674-1056/abd2ad

1. Introduction

The recent observation of an ultradilute self-bound droplet-like state[1] in single-component dipolar Bose–Einstein condensates (BECs)[2–5] and binary Bose–Bose mixtures[6–11] opens an entirely new direction to better understand the fascinating concept of quantum droplets — autonomously isolated quantum systems equilibrated under zero pressure in free space. Quantum droplets such as helium nano-droplets have already been intensively investigated in condensed matter community over the past few decades.[12–14] However, an in-depth understanding of helium nano-droplets is still lacking, due to the strong inter-particle interactions and the limited techniques to control and characterize the nano-droplets. These limitations could be overcome for ultradilute Bose droplets, owing to the unprecedented controllability in cold-atom experiments.[15] For example, the inter-particle interactions in Bose droplets can be tuned at will by using Feshbach resonances[16] and their structure and collective excitations can be accurately measured through *in-situ* or time-of-flight absorption imaging.[15] In particular, the realization of a weakly interacting Bose droplet now allows us to develop quantitative descriptions and makes it possible to have testable theoretical predictions.[17–36]

In this respect, it is worth noting the seminal work by Petrov,[17] where the existence of a Bose droplet is proposed in binary Bose mixtures with attractive inter-species attractions. The mean-field collapse is surprisingly shown to be arrested by an effective repulsive force arising from Lee–Huang–Yang (LHY) quantum fluctuations.[38] This ground-breaking proposal is now successfully confirmed in several experimental setups, including the homonuclear ^{39}K–^{39}K mixtures[6–9] and heteronuclear ^{41}K–^{87}Rb[10] or ^{23}Na–^{87}Rb mixtures.[11] Following Petrov's pioneering idea,[17] numerous theoretical investigations have been recently carried out,[17–27,29–37] addressing various zero-temperature properties of Bose droplets.

The finite-temperature properties of Bose droplets in both dipolar BECs and binary Bose mixtures, however, do not receive too much attention. Ultradilute droplets of dipolar bosons at finite temperature have recently been considered in the presence of an external harmonic trap.[28] For Bose droplets in binary mixtures, only the bulk properties (of an infinitely large droplet) at nonzero temperature are addressed most recently.[39,40] As the effective repulsive force provided by the LHY fluctuation term can be easily neutralized by thermal fluctuations, it is not a surprise to find that a Bose droplet in binary mixtures can be completely destabilized above a threshold temperature $T_{\rm th}$.[39]

The less interest in the finite temperature effect is probably due to the peculiar self-evaporation feature of quantum droplets. As a self-bound entity, the energy of elementary

*Project supported by the Australian Research Council's (ARC) Discovery Program (Grant Nos. DE180100592 and DP190100815), (Grant No. DP180102018), and (Grant No. DP170104008).

†Corresponding author. E-mail: hhu@swin.edu.au

excitations of quantum droplets – either single-particle excitations or collective excitations – has to be bounded from above by the so-called particle-emission threshold, making the droplet essentially a low-temperature object. This is fairly evident in helium nano-droplets: once the nano-droplet is created, its temperature rapidly decreases to about 0.4 K in several milliseconds.[13] Afterward, however, the self-evaporation becomes not so efficient.[13] A Bose droplet in a binary mixture is similarly anticipated to be a low-temperature object. In particular, as predicted by Petrov from zero-temperature calculations,[17] for the number of particles in a certain range, there are no collective excitations below the particle-emission threshold. In other words, an excitation-forbidden region in the particle number exists. The Bose droplet then may automatically lose its thermal energy upon releasing the most energetic particles and reach exactly zero temperature.

In this work, we would like to argue that the self-evaporation efficiency of Bose droplets at low temperature could be much reduced, as in helium nano-droplets.[13] As a result, the experimentally observed Bose droplets might have a small but nonzero temperature in the realistic timescale of experiments.[6–9] We theoretically determine the finite-temperature structure and collective excitations of self-bound spherical Bose droplets with a finite number of particles, based on time-independent and time-dependent extended Gross–Pitaevskii equations (GPEs),[17] respectively. We find a rich phase diagram at finite temperature. In particular, the excitation-forbidden, self-evaporation region of the Bose droplet, found earlier by Petrov using a zero-temperature theory,[17] turns out to shrink with increasing temperature and disappears eventually. We also predict that the surface modes and compressional sound modes of the Bose droplet become softened at the droplet-to-gas transition upon increasing temperature. Our results could be experimentally examined in binary Bose mixtures if efficient thermometry can be established at low temperatures.

2. Extended Gross–Pitaevskii equation at finite temperature

To address the finite-temperature properties of a finite-size Bose droplet, we consider the finite-temperature version of the extended GPE

$$\mathrm{i}\hbar\frac{\partial\Phi}{\partial t}=\left[-\frac{\hbar^2}{2m}\nabla^2-\mu+\frac{\partial\mathcal{F}}{\partial n}\left(n=|\Phi|^2\right)\right]\Phi, \tag{1}$$

where $\Phi(\boldsymbol{x},t)$ can be treated as the wave-function of the Bose droplet with atomic mass m, μ is the chemical potential to be determined by the total number of particles N, and $\mathcal{F}(n)$ is the local free energy functional (per unit volume $\mathcal{V}$) depending on the local density $n(\boldsymbol{x},t)=|\Phi(\boldsymbol{x},t)|^2$.

The extended GPE in the form of Eq. (1) was first used by Petrov in his seminal work as an effective phenomenological theory to describe the low-energy dynamics of an LHY droplet at zero temperature.[17] In the studies of helium nano-droplets, such a density-functional description is widely adopted.[12] For an overview, we refer to the review paper.[13] The microscopic derivation of the extended GPE Eq. (1) is difficult, due to an intrinsic in-consistency in Petrov's theory of the LHY droplet: one needs to artificially remove a small imaginary part in the LHY energy functional, which is related to the instability of mean-field collapse.[17] This difficulty was recently overcome by the present authors, with the consideration of the inter-species pairing of two bosons in different hyperfine states.[33,34] As a result of the correct description for the ground state, the extended GPE can be microscopically derived. This was demonstrated in our recent work for the zero-temperature case under the local density approximation.[35] The generalization of the derivation to the nonzero temperature $T\neq 0$ case is straightforward. We can simply replace the ground-state energy functional $\mathcal{E}(n)$ at zero temperature used in our previous work[35] with a finite-temperature energy function $\mathcal{F}(n)$ for free energy.

From the previous work for the finite-temperature bulk properties of the LHY droplet,[39] it is easy to show that the free energy functional per unit volume takes the form

$$\begin{aligned}\mathcal{F}=&-\frac{\pi\hbar^2}{m}\left(a+\frac{a^2}{a_{12}}\right)n^2+\frac{256\sqrt{\pi}}{15}\left(\frac{\hbar^2a^{5/2}}{m}\right)n^{5/2}\\&-\frac{\sqrt{\pi}}{720}\left(\frac{m^3k_{\mathrm{B}}^4T^4}{\hbar^6a^{3/2}}\right)n^{-3/2}\tilde{s}_3\left(1,\gamma\right),\end{aligned} \tag{2}$$

where $a>0$ and $a_{12}\simeq -a$ are the intra-species and inter-species s-wave scattering lengths of the binary Bose mixture, respectively. At zero temperature, the last term in the above expression is absent and the the free energy functional $\mathcal{F}(n)$ reduces to the ground-state energy functional $\mathcal{E}(n)$.[17] We then recover the zero-temperature extended GPE that has been extensively used in the literature. The last term accounts for the finite-temperature effect and the function $\tilde{s}_3[1,\gamma\equiv mk_{\mathrm{B}}T/(2\pi\hbar^2an)]$ could be calculated numerically.[39] It becomes unity in the zero-temperature limit and decreases with increasing temperature.[39] It turns out that close to the threshold for the formation of Bose droplets, i.e., $a_{12}\simeq -a$, the function $\tilde{s}_3(1,\gamma)$ could be reasonably approximated by an exponential decay form at low temperature, i.e.,

$$s_3\left(1,\gamma\right)\simeq\exp\left(-A\gamma\right), \tag{3}$$

with a decay constant $A\simeq 0.5$. This is shown in Fig. 1(a), where the predictions of Eqs. (2) and (3) are compared with the numerical results from the bosonic pairing theory.[39] Equation (2) also enables us to calculate the pressure by using

the standard thermodynamic relation, $P = n^2[\partial(\mathcal{F}/n)/\partial n]$. It is evident from Fig. 1(b) that the zero-pressure condition, which is required for a self-bound Bose droplet, can not be satisfied for relatively large temperature (i.e., $T = 1.5 \times 10^{-4}\hbar^2/(2ma^2)$). Indeed, from the analysis of our previous work,[39] we find that an infinitely large Bose droplet thermally dissolves itself once the temperature is above a threshold

$$k_{\rm B}T_{\rm th} \simeq 0.0222\left(1+\frac{a}{a_{12}}\right)^2\frac{\hbar^2}{ma^2}. \tag{4}$$

For the inter-species interaction strength considered in Fig. 1, $a_{12} = -1.05a$, the threshold temperature is about $k_{\rm B}T_{\rm th} \simeq 5.03\times10^{-5}\hbar^2/(ma^2)$. To be specific, we will concentrate on this example with $a_{12} = -1.05a$. But, it will become clear later that our results do not depend on this particular choice of the interaction parameters.

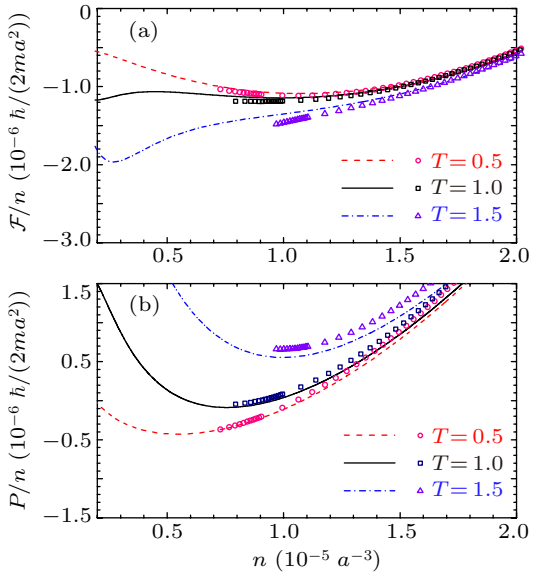

Fig. 1. Equation of state (EoS). The free energy per particle $\mathcal{F}/n$ (a) and pressure per particle P/n (b) of a homogeneous binary Bose mixture, in units of $10^{-6}\hbar^2/(2ma^2)$, are shown as a function of the density n at three temperatures $k_{\rm B}T = 0.5$, 1.0, and 1.5. The density n and temperature T are measured in units of $10^{-5}a^{-3}$ and $10^{-4}\hbar^2/(2ma^2)$, respectively. A self-bound Bose droplet is realized, when the pressure is zero at an equilibrium density n_0. The symbols and lines show the numerical and analytical results, respectively. The former is from a bosonic pairing theory, while the latter is calculated according to Eqs. (2) and (3). We note that the numerical results are not available at sufficiently low density. Here, we consider the inter-species interaction strength $a_{12} = -1.05a$.

It is useful to note that an exponential decay form of the function $\tilde{s}_3(1,\gamma)$ is very helpful for our numerical solutions of the extended GPE. This exponential decay, i.e., $e^{-B/n}$ with $B \equiv Amk_{\rm B}T/(2\pi\hbar^2 a)$, largely compensates the power-law increase $n^{-3/2}$ in the last term of the free energy Eq. (2) at low density and therefore removes the possible numerical instability caused by the sufficiently low density at the edge of the Bose droplet.

To ease the numerical workload, it is also helpful to use the (dimensionless) re-scaled coordinate and time as suggested by Petrov in his pioneering work[17]

$$\tilde{\boldsymbol{x}} = \frac{\boldsymbol{x}}{\xi}, \tag{5}$$

$$\tilde{t} = \frac{t}{m\xi^2/\hbar}, \tag{6}$$

$$\phi = \frac{\Phi}{\sqrt{n_0}}, \tag{7}$$

$$\tilde{\mu} = \frac{\mu}{\hbar^2/(m\xi^2)}, \tag{8}$$

where the equilibrium (bulk) density n_0 of a large Bose droplet at zero temperature is[33]

$$n_0 \equiv \frac{25\pi}{16384}\left(1+\frac{a}{a_{12}}\right)^2 a^{-3}, \tag{9}$$

and the length scale ξ can be chosen in such a way that the ground-state energy functional (i.e., the free energy functional at zero temperature) per unit volume takes the form $\mathcal{E} = -3|\phi|^4/2 + |\phi|^5$.[17] This leads to the energy scale

$$\frac{\hbar^2}{m\xi^2} = \frac{25\pi^2}{24576}\left(1+\frac{a}{a_{12}}\right)^3\frac{\hbar^2}{ma^2}. \tag{10}$$

At $a_{12} = -1.05a$, we find the energy units $\hbar^2/(m\xi^2) \simeq 1.08\times10^{-6}\hbar^2/(ma^2)$ and the units for the number of particles $n_0\xi^3 = N/\tilde{N} \simeq 9630$, where $\tilde{N}$ is the reduced number of particles. In terms of the energy scale $\hbar^2/(m\xi^2)$, we may re-write the threshold temperature as

$$k_{\rm B}T_{\rm th} \simeq 2.21\left(1+\frac{a}{a_{12}}\right)^{-1}\frac{\hbar^2}{m\xi^2}, \tag{11}$$

which is about $46.4\hbar^2/(m\xi^2)$ at $a_{12} = -1.05a$.

From now on, without any confusion we shall remove the tilde above the re-scaled quantities. The time-dependent extended GPE then takes the following dimensionless form:

$$\mathrm{i}\frac{\partial}{\partial t}\phi = \left[-\frac{1}{2}\nabla^2 - \mu + \frac{\partial\mathcal{F}}{\partial n}(\phi,\phi^*)\right]\phi, \tag{12}$$

where the dimensionless free energy functional is now given by (the density $n = |\phi|^2$)

$$\mathcal{F} = -\frac{3}{2}|\phi|^4 + |\phi|^5 - \frac{C_T}{|\phi|^3}\exp\left[-\frac{B_T}{|\phi|^2}\right], \tag{13}$$

with the temperature-dependent constants

$$C_T \equiv \frac{\pi^4}{62208}\left[\frac{(1+a/a_{12})k_{\rm B}T}{\hbar^2/(m\xi^2)}\right]^4 \simeq 0.0374\frac{T^4}{T_{\rm th}^4}, \tag{14}$$

$$B_T \equiv \frac{A}{3}\left(1+\frac{a}{a_{12}}\right)\frac{k_{\rm B}T}{\hbar^2/(m\xi^2)} \simeq 0.369\frac{T}{T_{\rm th}}. \tag{15}$$

At zero temperature, where the last term in Eq. (13) is absent, Eq. (12) recovers the dimensionless extended GPE used earlier by Petrov.[17] The two temperature-dependent constants C_T and B_T are the functions of the ratio $T/T_{\rm th}$ only and do not depend explicitly on the scattering lengths a and a_{12}. Near

the threshold temperature $T \sim T_{\rm th}$, both constants become significant, and we find that the LHY quantum-fluctuation term ($\propto |\phi|^5$) in the free energy functional is largely compensated by the last thermal-fluctuation term. This eventually destabilizes a large Bose droplet at the threshold temperature $T_{\rm th}$.[39] Let us now analyze how does this thermal destabilization occur for a Bose droplet with a finite (reduced) number of particles.

2.1. Time-independent GPE for the density distribution ϕ_0

In free space, the self-bound Bose droplet takes an isotropic spherical profile, depending on the radius r only.[8,17] The static profile $\phi_0(r) \geq 0$ at finite temperature satisfies the time-independent version of Eq. (12)

$$\hat{\mathcal{L}}\phi_0(r) = \mu\phi_0(r), \tag{16}$$

where we have defined the operator

$$\hat{\mathcal{L}} \equiv -\frac{\nabla^2}{2} - 3\phi_0^2 + \frac{5}{2}\phi_0^3 + \frac{\partial \mathcal{F}_T}{\partial n}. \tag{17}$$

The last term of the thermal contribution to $\hat{\mathcal{L}}$ is explicitly given by

$$\frac{\partial \mathcal{F}_T}{\partial n} = +\frac{3C_T}{2\phi_0^5}\left(1 - \frac{2B_T}{3\phi_0^2}\right)\exp\left[-\frac{B_T}{\phi_0^2}\right]. \tag{18}$$

In this work, we solve the static GPE numerically via a gradient method, which improves the accuracy and efficiency from our previous work.[15,41,42] The details of our numerical method are described in Appendix A.

2.2. Bogoliubov equations for collective excitations

To study the collective excitations of the Bose droplet, we consider small fluctuation modes around the condensate wave-function $\phi_0(r)$[15,32,42]

$$\phi(\boldsymbol{x},t) = \phi_0(r) + \sum_j \left[u_j(\boldsymbol{x})\,\mathrm{e}^{-\mathrm{i}\omega_j t} + v_j^*(\boldsymbol{x})\,\mathrm{e}^{+\mathrm{i}\omega_j t}\right], \tag{19}$$

where different mode with mode frequency ω_j is indexed by an integer j, and $u_j(\boldsymbol{x})$ and $v_j(\boldsymbol{x})$ are the corresponding mode wave-functions. For a spherical droplet, the index j can be further denoted by two good quantum numbers (l,n), where l is the angular momentum and n stands for the radial quantum number (i.e., the number of nodes in the radial wave-function). By substituting the above expression into the dimensionless extended GPE Eq. (12) and expanding it to the linear order in $u_j(\boldsymbol{x})$ and $v_j(\boldsymbol{x})$, we obtain the celebrated Bogoliubov equations[15,32,42]

$$\begin{bmatrix} \hat{\mathcal{L}} - \mu + \hat{\mathcal{M}} & \hat{\mathcal{M}} \\ \hat{\mathcal{M}} & \hat{\mathcal{L}} - \mu + \hat{\mathcal{M}} \end{bmatrix} \begin{bmatrix} u_j(\boldsymbol{r}) \\ v_j(\boldsymbol{r}) \end{bmatrix} = \omega_j \begin{bmatrix} +u_j(\boldsymbol{r}) \\ -v_j(\boldsymbol{r}) \end{bmatrix}, \tag{20}$$

where the operator $\hat{\mathcal{M}}$ is given by

$$\hat{\mathcal{M}} \equiv n\frac{\partial^2 \mathcal{F}}{\partial n^2} = -3\phi_0^2 + \frac{15}{4}\phi_0^3 + n\frac{\partial^2 \mathcal{F}_T}{\partial n^2}, \tag{21}$$

and the explicit form of the last thermal term in $\hat{\mathcal{M}}$ is

$$n\frac{\partial^2 \mathcal{F}_T}{\partial n^2} = -\frac{15C_T}{4\phi_0^5}\left(1 - \frac{4B_T}{3\phi_0^2} + \frac{4B_T^2}{15\phi_0^4}\right)\exp\left[-\frac{B_T}{\phi_0^2}\right]. \tag{22}$$

It should be noted that the wave-functions $u(\boldsymbol{x}) = +\phi_0(r)$ and $v(\boldsymbol{x}) = -\phi_0(r)$ are the zero-energy solution (i.e., $\omega_j = 0$) of the Bogoliubov equations. This is precisely the condensate mode of the Bose droplet and therefore should be discarded. To numerically solve the Bogoliubov equations, we follow the technique by Hutchinson, Zaremba, and Griffin.[43] The details of the numerical implementation can be found in Ref. [42] and Appendix A.

3. Results and discussion

For a given reduced number of particles N and a given reduced temperature (i.e., the ratio $T/T_{\rm th}$), we have numerically solved the dimensionless static GPE Eq. (16) and Bogoliubov equations Eq. (20) for the density distribution $\phi_0(r)$ and the collective excitation spectrum ω_j, respectively. To connect with the experimental observables at different scattering lengths a and a_{12}, we can restore the units of different quantities (i.e., density, mode frequency, and temperature) by simply multiplying, for example, the equilibrium density n_0, the energy scale $\hbar^2/(m\xi^2)$, and the temperature scale $T_{\rm th}$, which are given in Eqs. (9), (10), and (11), respectively.

In the following, we first consider the excitation spectrum at some chosen temperatures and determine a rich finite-temperature phase diagram. We then discuss in detail the temperature dependence of the density distribution and excitation spectrum at fixed number of particles, mimicking the realistic experimental measurements with running temperature.

3.1. Collective excitations at a given temperature

To start, let us briefly review the essential zero-temperature properties of a self-bound Bose droplet.[17] First, the chemical potential μ of the droplet has to be negative ($\mu < 0$), less than that of the surrounding vacuum (i.e., $\mu_{\rm vac} = 0$). Otherwise, it is not energetically favorable for particles to be added into the droplet. For an infinitely large droplet, where the edge effect can be safely neglected, it is clear from the stationary GPE Eq. (16) that the condensate wave-function in the bulk is $\phi_0 = 1$ in the re-scale units and the chemical potential $\mu = -1/2$. As we decrease the number of particles in the droplet, the wave-function $\phi_0(r)$ will be smaller than unity and the chemical potential increases towards $\mu \to 0^-$. The droplet will eventually become unstable and experience a droplet-to-gas transition, when the zero-pressure condition for the droplet state is strongly violated at low density. The droplet-to-gas transition at the critical number of particles $N_{\rm c} \simeq 18.65$ has

been analyzed in detail by Petrov,[17] by considering the balance between the kinetic energy (i.e., from the Laplace operator $-\nabla^2/2$) and the interaction energy (i.e., $\mathcal{F}(\phi_0)$). The transition is clearly signaled by the softening of the breathing mode frequency $\omega_{l=0,n=0}$, which vanishes precisely at N_c. This is shown by blue circles in Fig. 2(a), where we reproduce the lower panel of Fig. 1 in Ref. [17]. Petrov also predicted the existence of a metastable droplet state when the number of particles is slightly larger than the critical number, i.e., $N_c < N < N_m \simeq 22.55$.[17] This metastable state has a positive total energy, i.e., $-\mathcal{F} < 0$ as shown in Fig. 2(a), so the particles in the droplet will eventually escape to the vacuum via tunneling through an energy barrier (created by the competing kinetic and interaction energies).

Another interesting zero-temperature feature of the Bose droplet is the existence of an excitation-forbidden window in the number of particles,[17] as we mentioned earlier. In Fig. 2(a), there is no collective excitation in the stable droplet state below a threshold number of particles, $N < N_{th} \simeq 94.2$. All collective excitations are accumulated right above the particle-emission threshold $|\mu|$, forming an unbounded collective excitation continuum.[42] The bounded collective excitations are only possible at $N > N_{th}$, where the quadruple mode frequency $\omega_{l=2,n=0}$ first becomes smaller than $|\mu|$,[17] as shown by the red empty squares. At sufficiently large number of particles (i.e., $N \sim 10^4$), the Bose droplet is able to acquire a series of the surface modes and compressional sound modes with well-defined dispersion relations,[17,42] as we shall see later.

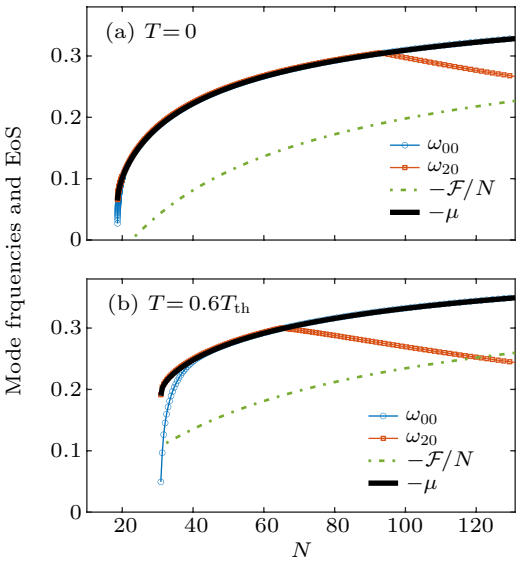

Fig. 2. The chemical potential $-\mu$, free energy per particle $-\mathcal{F}/N$, breathing mode frequency, and quadrupole mode frequency as a function of the number of particle at zero temperature (a) and at temperature $T = 0.6T_{th}$ (b). At zero temperature in (a), a metastable Bose droplet occurs when the number of particles decreases down to $N_m \simeq 22.55$, when the free energy $\mathcal{F}$ becomes positive (or $-\mathcal{F}$ becomes negative).

At finite temperature, the collective excitation spectrum can dramatically change. In Fig. 2(b), we report the excitation spectrum at $T = 0.6T_{th}$. It is readily seen that the droplet-to-gas transition now occurs at a much larger critical number of particles, $N_c(T = 0.6T_{th}) \simeq 30.9$, where the breathing mode frequency drops to zero. At the same time, the free energy $\mathcal{F}$ is always negative, indicating that the metastable droplet state found at zero temperature does not exist anymore. The threshold number of particle for the excitation-forbidden window also significantly decreases and we find that $N_{th}(T = 0.6T_{th}) \simeq 66.2$. For $N > 66.2$, the quadruple mode frequency ω_{20} decreases with increasing number of particles, while the breathing mode frequency ω_{00} continuously follows the particle-emission threshold $|\mu|$ at the number of particles considered in the figure.

In Fig. 3, we show the excitation spectrum at an even higher temperature $T = 0.8T_{th}$. At this temperature, the excitation-forbidden window in the number of particles completely disappears. Both the breathing mode frequency and quadruple mode frequency appear to be bounded below the particle-emission threshold $|\mu|$.

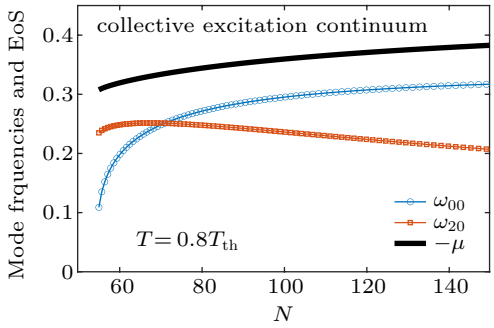

Fig. 3. The chemical potential $-\mu$, breathing mode frequency, and quadrupole mode frequency as a function of the number of particle at temperature $T = 0.8T_{th}$.

3.2. A finite-temperature phase diagram

We have calculated the excitation spectrum at different reduced temperatures and consequently have obtained a finite-temperature phase diagram, as reported in Fig. 4. This presents the main result of our work. Here, the critical number of particle N_c (black solid curve) is determined by extrapolating the breathing mode frequency ω_{00} to zero, and the critical number N_m (red dashed curve) is obtained by tracing the position where the free energy becomes positive. The two curves crosses with each other at about $0.24T_{th}$, above which the window for a metastable droplet state closes. It is interesting to note that the critical number of particles N_c shows a sensitive temperature dependence. It increases very rapidly once the temperature is above about $0.4T_{th}$. Approaching the bulk threshold temperature T_{th}, a Bose droplet with any number of particles becomes thermally unstable, as we already show in the previous work.[39]

On the other hand, the threshold number of particle $N_{\rm th}$ (blue dash-dotted curve) can be determined from the crossing point between the quadruple mode frequency ω_{20} and the particle-emission threshold $|\mu|$. It separates the phase space for a stable Bose droplet into two regimes: an excitation-forbidden droplet regime without any bounded collective excitations below the particle-emission threshold and a standard droplet regime with at least one discrete collective excitation. With increasing temperature, we find that the $N_{\rm th}$-curve terminates at about $0.73T_{\rm th}$ (see, i.e., the solid circle symbol in the figure). Above this temperature, we always find standard Bose droplets, in which a small but nonzero temperature or entropy could be accommodated by the discrete bounded collective excitations. Therefore, the intriguing self-evaporation phenomenon predicted by Petrov, i.e., the emission of particles upon arbitrary excitations,[17] ceases to exist. The Bose droplets then fail to automatically reach zero temperature.

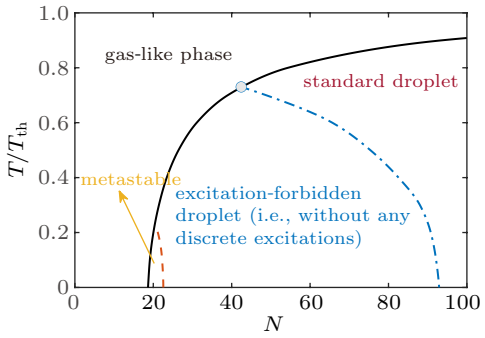

Fig. 4. The phase diagram of a finite-size Bose droplet as functions of the reduced number of particles N (horizontal axis) and of the reduced temperature $T/T_{\rm th}$ (vertical axis). At high temperature and small number of particles, the system is in the gas-like phase, while at low temperature and large number of particles, it is in the droplet state. A metastable droplet state also occurs at low temperature and relatively small number of particle.

3.3. The temperature-dependences of the density distribution and collective excitations

Let us now consider an idealized experimental situation. Initially, a Bose droplet is nearly in thermal equilibrium at a nonzero temperature. It then gradually reduces its temperature by emitting a very small portion of the most energetic particles. This slow self-evaporation might be treated as an adiabatic process. By taking the *in-situ* or time-of-flight absorption imaging of the Bose droplet, we may then experimentally extract the temperature-dependences of the density distribution and collective excitations of the Bose droplet at a nearly constant number of particles.

3.3.1. Large Bose droplets

In Fig. 5, we present the density distribution of a large Bose droplet with the number of particles $N = 3000$ at zero temperature (solid curve) and at $T = 0.7T_{\rm th}$ (dashed curve). For such a large droplet, the distribution acquires the typical flat-top structure.[17] Moreover, the temperature dependence of the density profile is not so apparent: the difference between the distributions at the two temperatures is less than 3%. This is correlated with a weak-temperature dependence of the droplet radius R, as shown in the inset, where the radius is defined as the square root of the mean square of the distance, $R = \sqrt{5\langle r^2\rangle/3}$. The droplet size only increases notably when the temperature is close to the bulk thermal destabilization threshold $T_{\rm th}$ (i.e., $T > T_{\rm th}$).

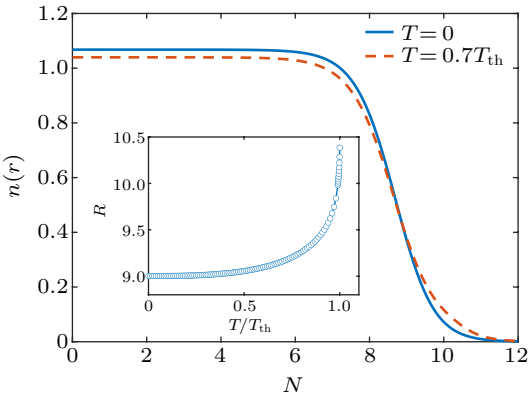

Fig. 5. The density distribution $n(r)$ of a large self-bound Bose droplet ($N = 3000$) at zero temperature (blue solid curve) and at the temperature $T = 0.7T_{\rm th}$ (red dashed curve). The inset shows the temperature dependence of the size of the Bose droplet, defined by $R = \sqrt{5\langle r^2\rangle/3}$.

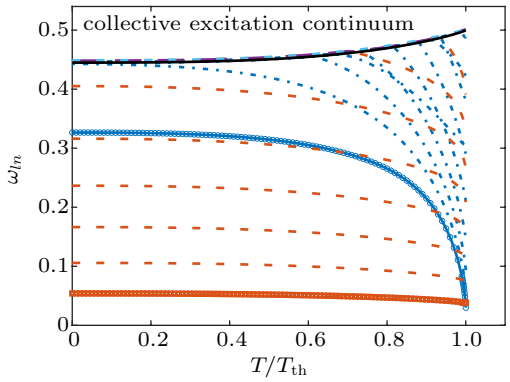

Fig. 6. Excitation frequencies ω_{ln} ($l \leq 9$ and $n \leq 2$) of a large self-bound Bose droplet ($N = 3000$), as a function of the reduced temperature $T/T_{\rm th}$. The red dashed curves show the surface modes $\omega_{l\geq 2,n=0}$ and the blue dash-dotted curves show the compressional bulk modes. The lowest surface mode ω_{20} (i.e, quadruple mode) and the lowest bulk mode (breathing mode) are highlighted by the red open squares and blue open circles, respectively. The black thick curve shows the threshold $-\mu$.

In Fig. 6, we report the corresponding collective excitation spectrum as a function of the temperature. At zero temperature, there are a number of discrete modes, which can be well categorized as the surface modes ($\omega_{l\geq 2,n=0}$, red open squares and red dashed curves) and bulk modes (ω_{00}, the breathing mode in blue circles; and $\omega_{l,n\neq 0}$, blue dash-dotted curves).[42] The surface modes only propagate near the edge of the Bose droplet and have an exotic dispersion relation $\omega_{l0}^{(\rm surface)} \propto \sqrt{\sigma_{\rm s} l(l-1)(l+2)}/R^{3/2}$, with $\sigma_{\rm s}$ being the surface tension.[13,17] In contrast, the bulk modes are compressional sound modes that propagate through the whole droplet

and have the standard dispersion relation $\omega_{ln}^{(\mathrm{bulk})} \propto c/R$, where c is the bulk sound velocity.[13,42] It is readily seen that the frequency of the low-lying surface modes does not change too much with increasing temperature. This could be understood from the robust flat-top and temperature insensitive density distribution as we observe in Fig. 5. As a result, the droplet size R, the surface tension σ_s, and hence the surface mode frequencies are less dependent on the temperature. On the other hand, the frequency of the bulk sound modes has a strong temperature dependence and clearly shows a waterfall-like effect close to the bulk threshold temperature T_{th}. The is related to the the softening of the sound velocity, which becomes exactly zero at the droplet-to-gas transition. All the bulk mode frequencies therefore have to vanish towards the transition.

3.3.2. Small Bose droplets

Let us now consider a Bose droplet with small reduced number of particles, which is more amenable to be created in the current experimental setups.[6,8] In Fig. 7, we show the density distribution of a $N = 100$ Bose droplet at two temperatures: $T = 0$ (solid curve) and $T = 0.7T_{\mathrm{th}}$ (dashed curve). Compared with a large Bose droplet in Fig. 5, the density distribution of a small droplet shows a more appreciable temperature dependence. In particular, the center density can change up to several tens of percent (see the inset), as we increase the temperature towards the threshold. This pronounced temperature dependence could be related to the loss of the flat-top structure in the density distribution due to the reduced number of particles. A small Bose droplet appears to be more easier to be altered than a large droplet.

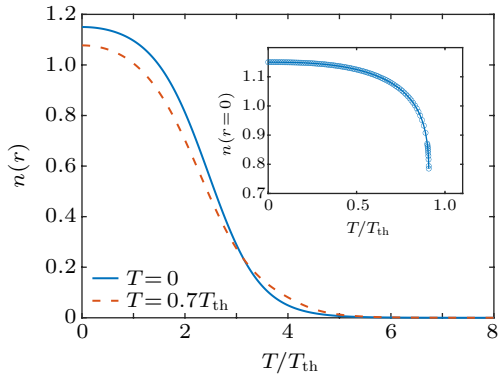

Fig. 7. The density distribution $n(r)$ of a small self-bound Bose droplet ($N = 100$) at zero temperature (blue solid curve) and at the temperature $T = 0.7T_{\mathrm{th}}$ (red dashed curve). The inset shows the temperature dependence of the center density at $r = 0$.

In Fig. 8, we report the temperature evolution of the collective excitation spectrum at $N = 100$. At this number of particles and at zero temperature, only the lowest surface mode (i.e., the quadruple mode ω_{20}) is bounded below the particle-emission threshold $|\mu|$.[17] When we increase the temperature, the quadruple mode frequency decreases notably, presumably due to the increase of the droplet radius, since the droplet at this size acquires a more sensitive temperature dependence as we mentioned earlier. Interestingly, at about $0.7T_{\mathrm{th}}$ the frequency of the lowest compression bulk mode, the breathing mode frequency, starts to fall off the particle-emission threshold. It becomes increasingly softened towards the threshold temperature T_{th}. At an even higher temperature (i.e., $T \sim 0.87T_{\mathrm{th}}$), more and more higher-order bulk modes fall off the the particle-emission threshold and become softened. This fall-off feature turns out to be very general, occurring also at smaller number of particles, as can be seen in the inset for the selected case of $N = 50$.

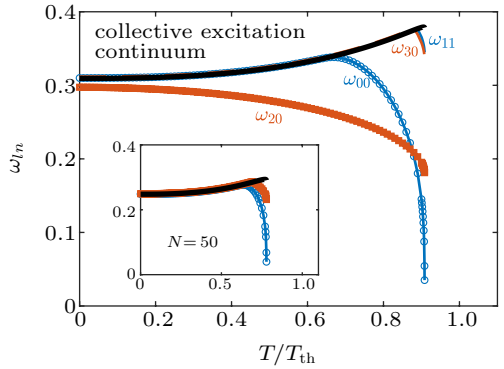

Fig. 8. Excitation frequencies ω_{ln} ($l \leq 9$ and $n \leq 2$) of a small self-bound Bose droplet ($N = 100$), as a function of the reduced temperature T/T_{th}. The red dashed curves show the surface modes $\omega_{l\geq 2,n=0}$ and the blue dash-dotted curves show the compressional bulk modes. The lowest surface mode ω_{20} (i.e, quadruple mode) and the lowest bulk mode (breathing mode) are highlighted by the red open squares and blue open circles, respectively. The black thick curve shows the threshold $-\mu$. At this number of particles, most of the excitation modes enter the collective excitation continuum with a frequency $\omega_{ln} \gtrsim -\mu$. The inset shows the excitation spectrum at an even smaller number of particles, $N = 50$.

The mode frequency softening, for both surface modes and compressional bulk modes in large and small Bose droplets, is therefore a characteristic feature of the thermally-induced droplet-to-gas transition at finite temperature. The mode softening effectively removes the excitation-forbidden interval in the number of particles predicted by Petrov at zero temperature,[17] and opens the possibility to observe a small Bose droplet with non-zero temperature.

4. Conclusions

In summary, we have theoretically investigated the finite-temperature effects on the structure and collective excitations of an ultradilute quantum droplet in free space, formed in a binary Bose–Bose mixture with inter-species attractions near the mean-field collapse. Our calculations are based on the extended (time-dependent) Gross–Pitaevskii equation generalized to the finite-temperature case. The density distribution is determined by solving the static Gross–Pitaevskii equation, while the collective excitation spectrum is obtained by solving the coupled Bogoliubov equations.

We have found a rich finite-temperature phase diagram as a function of the number of particles in the droplet. In particular, the critical number of particles at the droplet-to-gas transition is found to depend sensitively on the temperature. The excitation-forbidden interval predicted by Petrov is shown to shrink with increasing temperature and disappears completely at about $0.73T_{\rm th}$, where $T_{\rm th}$ is the threshold temperature for thermally destabilizing an infinitely large Bose droplet. Above the temperature $0.73T_{\rm th}$, there is at least one discrete collective mode below the particle-emission threshold, which may block the self-evaporation of the Bose droplet and allow a small but nonzero temperature.

Our results could be experimentally examined, if we are able to overcome the difficulty of finding a useful thermometry to measure the temperature. Qualitatively, at the number of particles slightly below $N_{\rm th}(T=0)\simeq 94.2$, the experimental observation of discrete quadrupole mode frequency or breathing mode frequency below the particle-emission threshold, i.e., $\omega_{20}<|\mu|$ or $\omega_{00}<|\mu|$, would be a very strong evidence for the finite-temperature effect.

Appendix A: Numerical method

Here, we describe our numerical approach to find the ground state solution of the static extended GPE Eq. (16), which is equivalent to minimize an energy density functional $\mathcal{E}/N$, where $N=\int {\rm d}\boldsymbol{r}|\phi_0(\boldsymbol{r})|^2$. The energy functional in the free-space is given by

$$\mathcal{E}=\langle K\rangle+\langle\mathcal{F}\rangle, \tag{A1}$$

where

$$\langle K\rangle=-\frac{1}{2}\int {\rm d}\boldsymbol{r}\phi_0(\boldsymbol{r})\nabla^2\phi_0(\boldsymbol{r}), \tag{A2}$$

$$\langle\mathcal{F}\rangle=\int {\rm d}\boldsymbol{r}\mathcal{F}(\boldsymbol{r}). \tag{A3}$$

Here $\mathcal{F}(\boldsymbol{r})$ is given by Eq. (13), with $\boldsymbol{r}$-dependency explicitly written out.

Due to the spherical symmetry of the system, we only consider the s-wave solution ($l=0$). Therefore, equation (16) reduces to an effective 1D radial equation. We first expand the condensed wave function in a 5-th order B-splines basis[44]

$$\phi_0(\boldsymbol{r})=\frac{1}{\sqrt{4\pi}}\sum_n c_n\frac{b_n(r)}{r}. \tag{A4}$$

The B-spline basis has been extensively used in solving Schröinger equations in two- and three-body problems with high accuracy.[45,46] The B-spline basis allows us to use an uneven grid, which might better represent the solution wavefunction. The B-spline basis also allows a higher order approximation of the derivative operator that appears in the kinetic energy term. The energy density functional $\mathcal{E}/N$ then can be regarded as a non-linear function of coefficients c_n, which can be minimized using the standard conjugate-gradient method via software package such as "minFunc" in Matlab.[47]

References

[1] Bötcher F, Schmidt J N, Hertkorn J, Ng K S H, Graham S D, Guo M, Langen T and Pfau T 2020 arXiv:2007.06391
[2] Ferrier-Barbut I, Kadau H, Schmitt M, Wenzel M and Pfau T 2016 *Phys. Rev. Lett.* **116** 215301
[3] Schmitt M, Wenzel M, Böttcher F, Ferrier-Barbut I and Pfau T 2016 *Nature* **539** 259
[4] Chomaz L, Baier S, Petter D, Mark M J, Wächtler F, Santos L and Ferlaino F 2016 *Phys. Rev. X* **6** 041039
[5] Böttcher F, Wenzel M, Schmidt J-N, Guo M, Langen T, Ferrier-Barbut I, Pfau T, Bombín R, Sánchez-Baena J, Boronat J and Mazzanti F 2019 *Phys. Rev. Research* **1** 033088
[6] Cabrera C, Tanzi L, Sanz J, Naylor B, Thomas B, Cheiney P and Tarruell L 2018 *Science* **359** 301
[7] Cheiney P, Cabrera C R, Sanz J, Naylor B, Tanzi L and Tarruell L 2018 *Phys. Rev. Lett.* **120** 135301
[8] Semeghini G, Ferioli G, Masi L, Mazzinghi C, Wolswijk L, Minardi F, Modugno M, Modugno G, Inguscio M and Fattori M 2018 *Phys. Rev. Lett.* **120** 235301
[9] Ferioli G, Semeghini G, Masi L, Giusti G, Modugno G, Inguscio M, Gallemi A, Recati A and Fattori M 2019 *Phys. Rev. Lett.* **122** 090401
[10] D'Errico C, Burchianti A, Prevedelli M, Salasnich L, Ancilotto F, Modugno M, Minardi F and Fort C 2019 *Phys. Rev. Research* **1** 033155
[11] Wang D 2019 *Quantum Droplet in Heteronuclear Double Bose-Einstein Condensates*, talk at IAS Workshop on Quantum Simulation of Novel Phenomena with Ultracold Atoms (May 6–7, 2019)
[12] Dalfovo F, Lastri A, Pricaupenko L, Stringari S and Treiner J 1995 *Phys. Rev. B* **52** 1193
[13] Barranco M, Guardiola R, Hernández S, Mayol R, Navarro J and Pi M 2006 *J. Low Temp. Phys.* **142** 1
[14] Gessner O and Vilesov A F 2019 *Annu. Rev. Phys. Chem.* **70** 173
[15] Dalfovo F, Giorgini S, Pitaevskii L P and Stringari S 1999 *Rev. Mod. Phys.* **71** 463
[16] Chin C, Grimm R, Julienne P and Tiesinga E 2010 *Rev. Mod. Phys.* **82** 1225
[17] Petrov D S 2015 *Phys. Rev. Lett.* **115** 155302
[18] Petrov D S and Astrakharchik G E 2016 *Phys. Rev. Lett.* **117** 100401
[19] Baillie D, Wilson R M, Bisset R N and Blakie P B 2016 *Phys. Rev. A* **94** 021602
[20] Wächtler F and Santos L 2016 *Phys. Rev. A* **94** 043618
[21] Li Y, Luo Z, Liu Y, Chen Z, Huang C, Fu S, Tan H and Malomed B A 2017 *New J. Phys.* **19** 113043
[22] Cappellaro A, Macrì T and Salasnich L 2018 *Phys. Rev. A* **97** 053623
[23] Astrakharchik G E and Malomed B A 2018 *Phys. Rev. A* **98** 013631
[24] Cui X 2018 *Phys. Rev. A* **98** 023630
[25] Staudinger C, Mazzanti F and Zillich R E 2018 *Phys. Rev. A* **98** 023633
[26] Ancilotto F, Barranco M, Guilleumas M and Pi M 2018 *Phys. Rev. A* **98** 053623
[27] Parisi L, Astrakharchik G E and Giorgini S 2019 *Phys. Rev. Lett.* **122** 105302
[28] Aybar E and Oktel M Ö 2019 *Phys. Rev. A* **99** 013620
[29] Cikojević V, Markić L V, Astrakharchik G E and Boronat J 2019 *Phys. Rev. A* **99** 023618
[30] Chiquillo E 2019 *Phys. Rev. A* **99** 051601(R)
[31] Minardi F, Ancilotto F, Burchianti A, D'Errico C, Fort C and Modugno M 2019 *Phys. Rev. A* **100** 063636
[32] Tylutki M, Astrakharchik G E, Malomed B A and Petrov D S 2020 *Phys. Rev. A* **101** 051601(R)
[33] Hu H and Liu X J 2020 *Phys. Rev. Lett.* **125** 195302
[34] Hu H, Wang J and Liu X J 2020 *Phys. Rev. A* **102** 043301
[35] Hu H and Liu X J 2020 *Phys. Rev. A* **102** 043302
[36] Wang Y, Guo L, Yi S and Shi T 2020 *Phys. Rev. Research* **2** 043074
[37] Wang J B, Pan J S, Cui X and Yi W 2020 *Chin. Phys. Lett.* **37** 076701

[38] Lee T D, Huang K and Yang C N 1957 *Phys. Rev.* **106** 1135
[39] Wang J, Hu H and Liu X J 2020 *New J. Phys.* **22** 103044
[40] Ota M and Astrakharchik G E 2020 *SciPost Phys.* **9** 020
[41] Pu H and Bigelow N P 1998 *Phys. Rev. Lett.* **80** 1130
[42] Hu H and Liu X J 2020 *Phys. Rev. A* **102** 053303
[43] Hutchinson D A W, Zaremba E and Griffin A 1997 *Phys. Rev. Lett.* **78** 1842
[44] de Boor C R 1978 *A Practical Guide to Splines* (New York: Springer)
[45] van der Hart H W 1997 *J. Phys. B: At. Mol. Opt. Phys.* **30** 453
[46] Wang J and Greene C H 2010 *Phys. Rev. A* **82** 022506
[47] Schmidt M 2005 *minFunc: unconstrained differentiable multivariate optimization in Matlab*